# Chapter 2

# A traveling Wave based Primary and Backup Protection for MMC-MTDC Transmission System using Morphological Un-Decimated Wavelet Scheme

## 2.1 General

LCC based HVDC grids are generally preferred over HVAC grids to efficiently transfer large amount of electrical energy over long distances. Furthermore, HVDC systems can also be used for interconnecting synchronous as well as asynchronous AC grids. With the advent of IGBT power electronics switching devices, VSC based HVDC systems are preferred over LCC-HVDC for connecting offshore as well as onshore renewable energy sources to the AC grid. Now upgrading from point-to-point HVDC system, MTDC systems are most widely used in power transmission offering better power system control, redundancy, flexibility, and reliability [97].

In this chapter, a TW-based primary and backup protection scheme is proposed for the MTDC grid. The main contributions of the chapter are –

- A robust, noise-tolerant, and setting-less morphological un-decimated wavelet (MUDW)

based primary protection scheme for the MMC-MTDC system is proposed. It detects polarity and AT for the first TW at both terminals to discriminate between internal and external fault.

- A TW-based remote backup protection scheme is proposed using the principle of fault zone identification (forward external or backward external zone).

## 2.2 MMC-MTDC test system

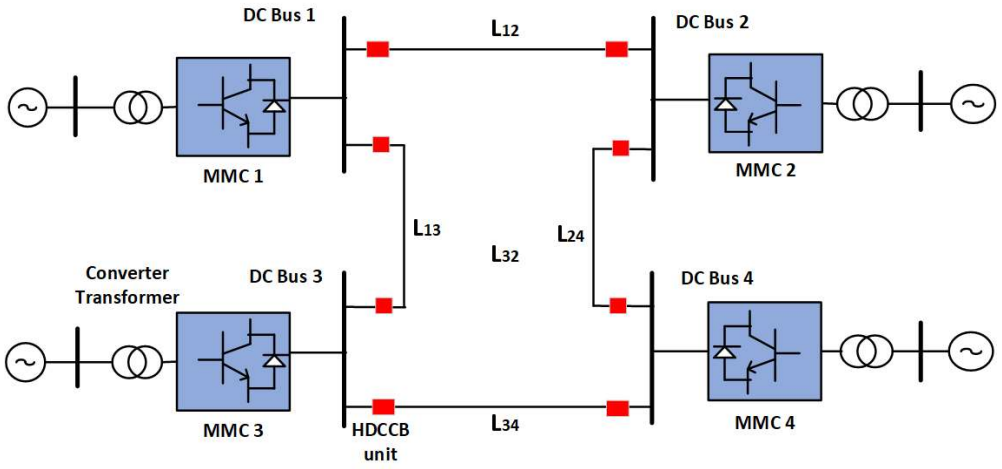


Figure 2.1: MMC-MTDC test grid system.

To start with, a four-terminal MMC-MTDC transmission system shown in Fig. 2.1 is described, which is used to test performance of the proposed protection scheme. Generally, the sampling frequency is kept in the range of a few hundred kHz for the TW-based protection scheme, therefore the sampling frequency is taken as 500 kHz for further analysis of performance of proposed protection scheme in this chapter. The MMC converters 2 and 4 are connected to two offshore AC wind farms (Thevenin AC source), whereas MMC converters 1 and 3 are connected to the onshore AC grid. The MMC-MTDC system has a symmetrical monopolar configuration and further details of the DC cable (link) and MMC converter parameters can be found in [98]. Moreover, the details of converter control model and HDCCB model can also be found in [98]. The MTDC grid and AC grid parameters are shown in Table 2.1. The test MMC-MTDC grid has two DC links ($L_{34}$ and $L_{12}$) of 200 km length and another two DC links ($L_{13}$ and $L_{24}$) of 100 km length.

Table 2.1: Parameters of MMC converter and AC/DC grid

| **Converter and grid parameters** | **Converter 1,2,3** | **Converter 4** |
|---|---|---|
| Rated power (MVA) | 900 | 1200 |
| AC grid voltage (kV) | 400 | 400 |
| DC grid voltage (kV) | ± 320 | ± 320 |
| AC converter voltage (kV) | 380 | 380 |
| AC grid reactance (Ω) | 17.7 | 13.4 |
| AC grid resistance (Ω) | 1.77 | 1.34 |
| Arm capacitance ($\mu F$) | 29.3 | 39 |
| Arm reactor (mH) | 84.8 | 63.6 |
| Arm resistance (Ω) | 0.885 | 0.67 |
| Bus filter reactor (mH) | 10 | 10 |

## 2.3 MUDW based primary and backup protection scheme for MTDC system

### 2.3.1 MUDW based TW polarity and AT detection

The mathematical morphology (MM) based protection scheme has been used in the MTDC system using multi resolution mathematical morphological gradient (MMG) technique to extract transient features from pole current/voltage signals [17]. Although the performance of MMG based protection scheme is quite satisfactory under different fault conditions, its performance deteriorates under noise-contaminated current/voltage signals. To overcome this issue, MUDW will be used to extract the polarity and AT of the TW from current signal instead of MMG, as MUDW is comparatively more noise-tolerant than the MMG technique. The various processes of extracting AT and polarity of the TW using MUDW is explained below -

1) **Pre-Processing of TW based relay input signal:**

Before obtaining the AT and polarity information of the fault-induced TW, modal transformation equation is used to essentially eliminate the mutual coupling effect of overhead DC transmission line or DC cable on the TW [30] -

$$\begin{bmatrix} i_{m0} \\ i_{m1} \end{bmatrix} = \frac{1}{\sqrt{2}} \begin{bmatrix} 1 & 1 \\ 1 & -1 \end{bmatrix}^{-1} \begin{bmatrix} i_p \\ i_n \end{bmatrix} \tag{2.1}$$

Here $i_{m0}$ and $i_{m1}$ are mode-0 and mode-1 current respectively, whereas $i_p$ and $i_n$ are current in positive and negative DC poles respectively. As clearly evident from (2.1) that $i_{m0}$ is zero during pole-to-pole (PP) fault and steady-state operation, but non-zero during positive-pole-to-ground (PPG) and negative-pole-to-ground (NPG). On the contrary, $i_{m1}$ is non-zero for PP, PPG as well as NPG fault. Therefore, mode-1 current is the chosen decoupled mode current to extract AT and polarity information of current TW.

2) **The theoretical background of MUDW, AT, and polarity extraction of TW:**

Signal decomposition schemes are essential to extract critical signal information. MM-based pyramid and coupled wavelet-based multi resolution decomposition scheme have been proposed in [99, 100]. Several levels are involved in the multi resolution decomposition scheme, where information quantity decreases towards a higher level. The analysis operator is used to reach a higher level whereas the synthesis operator is used to get to lower level.

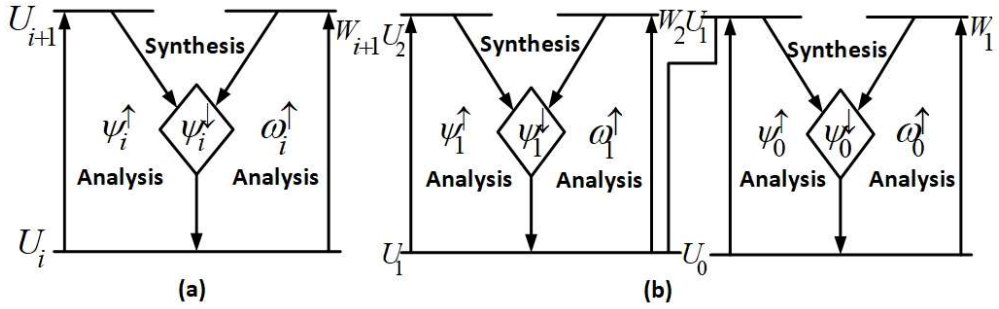


Figure 2.2: (a) Coupled wavelet decomposition scheme, (b) Two-level coupled wavelet decomposition scheme.

Consider a family of signal space $U_i$ and $i$ is a set of the finite or infinite index. There is a family of analysis operator $\psi_i^{\uparrow}$ mapping $U_i$ to $U_{i+1}$ and a family of synthesis operator $\psi_i^{\downarrow}$ mapping $U_{i+1}$ to $U_i$ as shown in Fig. 2.2(a). The analysis and synthesis operator

must satisfy the pyramid condition, i.e.; $\psi_i^{\uparrow}\psi_i^{\downarrow} = i_d$ and $i_d$ is an identity operator, which guarantees zero information loss in consecutive synthesis and analysis operations. Coupled wavelets are formulated on the principle of pyramid condition utilizing two analysis (signal analysis and detail analysis) and one synthesis operator, which is demonstrated in Fig. 2.2(a). In Fig. 2.2(a), $U_i$ is the set of signals at level $i$ and $W_i$ is the set of detail signals at level $i$; $\psi_i^{\uparrow}$, $\psi_i^{\downarrow}$, $\omega_i^{\uparrow}$ are signal analysis, synthesis, and detail analysis operators respectively and their details can be found in [99, 100] and further details are given in Appendix A.. The proposed protection scheme uses two stages, i.e.; $i = 2$, of coupled wavelet MUDW scheme along with un-decimated algorithm as shown in Fig. 2.2(b).

The un-decimated algorithm in MUDW ensures no decimation, i.e.; removes down-sampling and up-sampling in forward and inverse wavelet transform respectively. Hence it guarantees better quality filtering and no information loss with less distortion which may be caused by noise removal from the signal. The signal analysis, detail analysis, and synthesis operators can be mathematically written as –

$$\psi_i^{\uparrow}(x_i) = 0.5(\delta\gamma - \varepsilon\phi + \delta - \varepsilon)(x_i) = x_{i+1} \tag{2.2}$$

$$\omega_i^{\uparrow}(x_i) = \left[i_d - 0.5(\delta\gamma - \varepsilon\phi + \delta - \varepsilon)\right](x_i) = y_{i+1} \tag{2.3}$$

$$\psi_i^{\downarrow}(x_{i+1}, y_{i+1}) = i_d(x_i) = x_{i+1} + y_{i+1} \tag{2.4}$$

$$\psi_i^{\uparrow}(\psi_i^{\downarrow}(x_{i+1}, y_{i+1})) = \psi_i^{\uparrow}(i_d(x_i)) = x_{i+1} \tag{2.5}$$

We can also obtain that $\omega_i^{\uparrow}(\psi_i^{\downarrow}(x_{i+1}, y_{i+1})) = y_{i+1}$, whereas $x_i \in U_i$, $x_{i+1} \in U_{i+1}$, $y_{i+1} \in W_{i+1}$. Furthermore,

$$\psi_i^{\downarrow}(\psi_i^{\uparrow}(x_i), \omega_i^{\uparrow}(x_i)) = 0.5(\delta\gamma - \varepsilon\phi + \delta - \varepsilon)(x_i) + \left[i_d - 0.5(\delta\gamma - \varepsilon\phi + \delta - \varepsilon)\right](x_i) = x_i \tag{2.6}$$

The analysis and synthesis operator can be simply constructed using morphological dilation, erosion, opening, and closing operators denoted by $\delta$, $\varepsilon$, $\gamma$, and $\phi$ respectively as explained in [99, 100]. Hence, the MUDW decomposition scheme can also be written as –

$$\psi_i^{\uparrow} = 0.5(\delta\gamma - \varepsilon\phi + \delta - \varepsilon) = 0.5(\delta\varepsilon + \varepsilon\delta)(\delta - \varepsilon) \tag{2.7}$$

As evident from the above mathematical expression of MUDW decomposition, $(\delta - \varepsilon)$ signifies morphological gradient operator and $0.5(\delta\varepsilon + \varepsilon\delta)$ component is responsible for

noise suppression. Based on the above mathematical expression of the signal analysis operator of the MUDW scheme, the $n^{th}$ output level can be expressed as –

$$s_n = 2^{-n}(\delta\varepsilon + \varepsilon\delta)^n(\delta - \varepsilon)^n[i_{m1}(t)] \tag{2.8}$$

For n=2, the signal analysis operator is given as

$$s_2 = 0.25(\delta\varepsilon + \varepsilon\delta)^2(\delta - \varepsilon)^2[i_{m1}(t)] \tag{2.9}$$

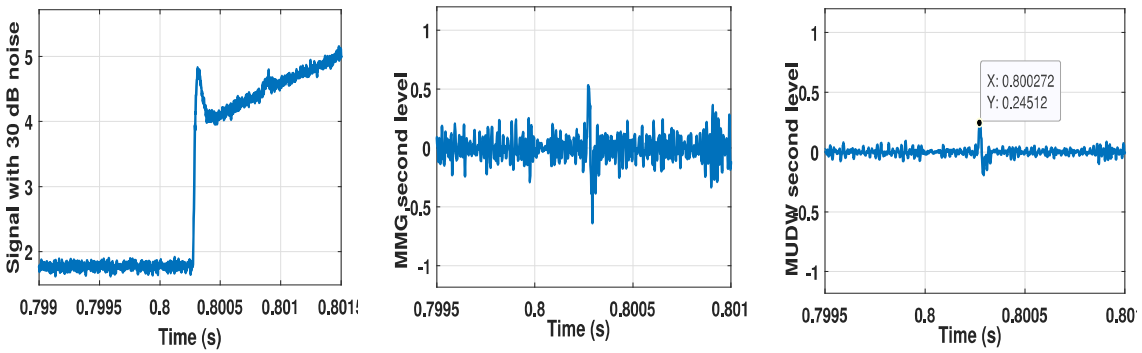


(a) (b) (c)

Figure 2.3: (a) Measurement signal with 30 dB noise, (b) MMG output, (c) MUDW output.

The component $(\delta - \varepsilon)^2$ in the above mathematical expression is the quadratic morphological gradient for mode-1 current $i_{m1}(t)$ and second level of MUDW decomposition scheme with flat structural element (SE) of the length of 4 sampling points is considered for the proposed protection scheme. The performance of second level MUDW is compared with second level MMG for extracting TW contaminated with 30 dB noise as shown in Fig. 2.3. As evident from Fig. 2.3, MUDW extracts AT (0.800272 s) and positive polarity of the TW, but MMG could not differentiate between noise and TW.

### 2.3.2 Principle of TW based primary and backup protection scheme

The protection unit layout of the substation $i$ is shown in Fig. 2.4(a). As shown in Fig. 2.4(a), the DC bus $i$ is connected to the MMC converter $i$ through a HDCCB unit $CB_i$. Bus $i$ is further connected to other $i_N$ numbers of buses through HDCCB unit $CB_1$, $CB_2$, $CB_3$.... $CB_N$. The current transducers (CTs) placed at the end of

each HVDC link ($CT_{13}$, $CT_{31}$, $CT_{34}$, $CT_{43}$, and so on) will measure DC pole current and send the measured signal to the data processing unit (DPU) of the substation protection system unit, where the MUDW signal processing technique is used to determine AT and polarity of the current TW. It also receives the AT and polarity information of the current TW from the neighboring substation via an intra substation optical fiber communication link or ethernet communication link conforming to IEC 61850 communication protocol [93, 95, 101]. Depending on the AT and polarity information of the current TW from the substation $i$ and its neighboring substation, three zones are created, i.e.; internal zone ($Z_{in}$), forward external zone ($Z_{fe}$), and backward external zone ($Z_{be}$). For instance, the test MMC-MTDC system shown in Fig. 2.1 has been redrawn as shown in Fig.2.4(c), with consideration of PP fault $F_1$ in DC transmission link ($L_{34}$). And the internal, forward external, and backward external zone for $L_{34}$ will be $Z_{34}^{in}$, $Z_{34}^{fe}$ and $Z_{34}^{be}$ respectively. Similarly, different zones are created for the DC transmission line as shown in Fig. 2.4(c). As evident from Fig. 2.4(c), each DC transmission line is covered under its own internal zone and forward external & backward external zone of the neighboring DC transmission line. For example, the DC link $L_{34}$ is covered by internal zone ($Z_{34}^{in}$), forward external zone ($Z_{13}^{fe}$), and backward external zone ($Z_{42}^{be}$).

The principle of the proposed primary and backup protection scheme is further explained as follows –

1) **Internal Fault zone (Primary Protection zone, $Z_{34}^{in}$):**

As shown in Fig. 2.4(c), for fault $F_1$ at a distance $xl_{34}$ from substation 3, the fault inception time is indicated by $t_0$. The AT of initial TW to $CT_{34}$ and $CT_{43}$ is

$$t_{34} = t_0 + \frac{xl_{34}}{v_{TW}} \tag{2.10}$$

$$t_{43} = t_0 + \frac{(1-x)l_{34}}{v_{TW}} \tag{2.11}$$

Here $t_{34}$ and $t_{43}$ show the AT of initial TW to $CT_{34}$ and $CT_{43}$ respectively. The total length of the DC transmission link $L_{34}$ is given by $l_{34}$, $x$ is the per unit value and $v_{TW}$ is the velocity of TW in the transmission line. By combining the above equations, we get

$$t_{34} - t_{43} = \frac{(2x-1)l_{34}}{v_{TW}} \tag{2.12}$$

Since $0 \leq x \geq 1$, it can be concluded that

$$|t_{34} - t_{43}| < \frac{l_{34}}{v_{TW}} \tag{2.13}$$

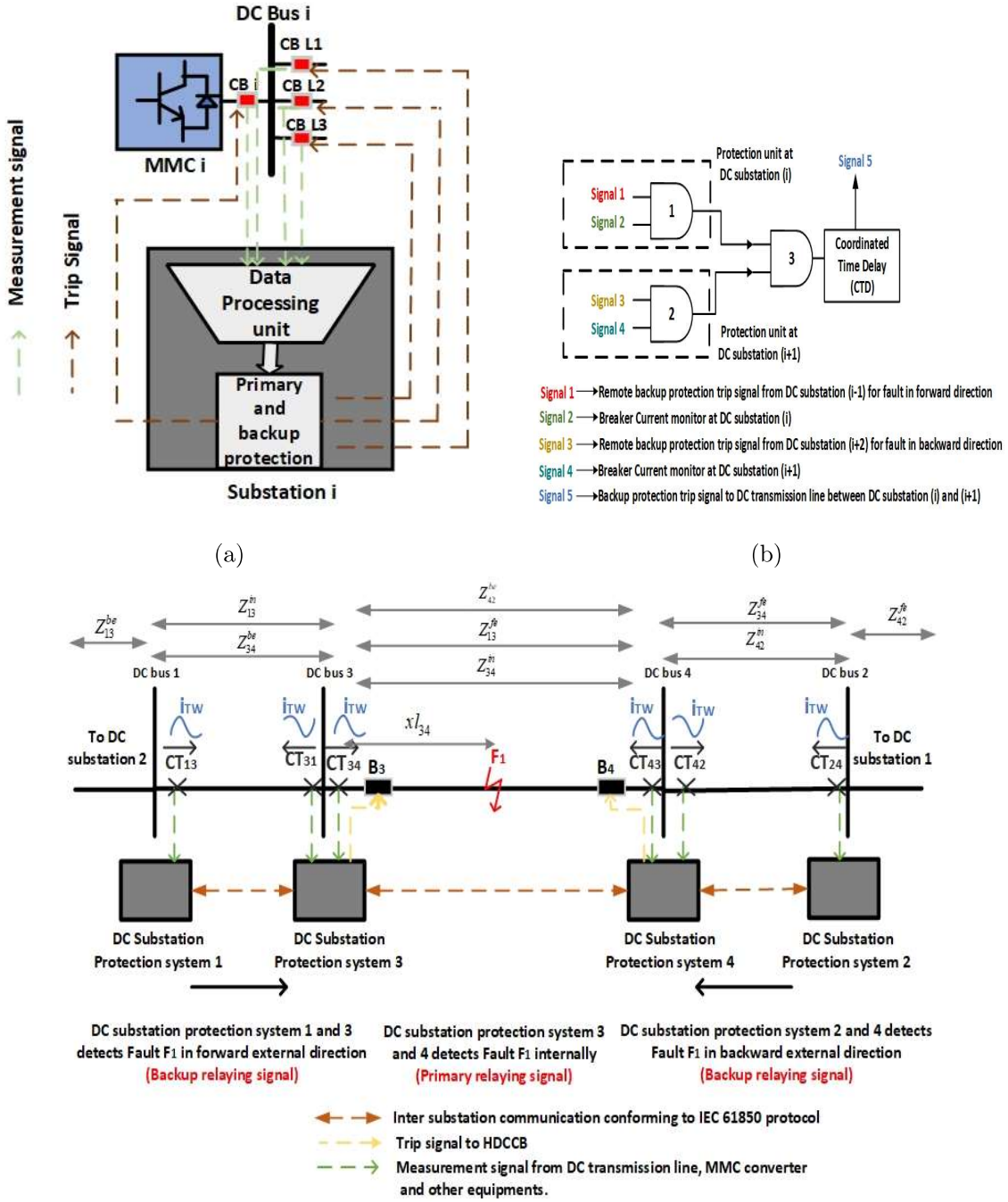


Figure 2.4: (a) DC substation protection unit layout, (b) Backup Protection logic diagram, (c) Proposed primary and backup protection scheme.

The polarity of TW for internal and external fault location is shown in Fig. 2.4(c) which is well explained in [30]. The convention for the direction of OCT ($CT_{13}, CT_{31}, CT_{34}$ and so on) are set to face towards the relay's respective internal protection zone. This convention simplifies polarity determination of current TW. For internal fault ($F_1$), the $CT_{34}$ and $CT_{43}$ sees fault in forward direction and therefore the polarity of the current TW is same for $CT_{34}$ and $CT_{43}$ [30].

$$P_{CT_{34}}.P_{CT_{43}} = 1 \tag{2.14}$$

2) **Forward External Zone (Backup Protection Zone, $Z_{13}^{fe}$):**

The fault ($F_1$) induced TW will travel further to DC link $L_{13}$ after crossing $CT_{34}$. The AT of fault ($F_1$) induced TW at the current transducers $CT_{13}$ and $CT_{31}$ is given as –

$$t_{13} = t_0 + \frac{l_{13}}{v_{TW}} + \frac{xl_{34}}{v_{TW}} \tag{2.15}$$

$$t_{31} = t_0 + \frac{xl_{34}}{v_{TW}} \tag{2.16}$$

Here $l_{13}$ is the length of the DC transmission link $L_{13}$. By combining the above equations, we get

$$t_{13} - t_{31} = \frac{l_{13}}{v_{TW}} \tag{2.17}$$

For fault $F_1$, $CT_{13}$ will see fault in forward and $CT_{31}$ will see fault in reverse direction. Therefore, the fault induced current TW at $CT_{13}$ and $CT_{31}$ will have opposite polarity [30]. Therefore,

$$P_{CT_{13}}.P_{CT_{31}} = -1 \tag{2.18}$$

Hence, the fault will be in the forward direction if equations (2.17) and (2.18) are satisfied.

3) **Backward External Zone (Backup Protection Zone, $Z_{42}^{be}$):**

The fault ($F_1$) induced TW will travel further to DC link $L_{42}$ after crossing $CT_{42}$. The AT of the TW at the relay $CT_{42}$ and $CT_{24}$ due to fault $F_1$ is given as –

$$t_{42} = t_0 + \frac{(1-x)l_{34}}{v_{TW}} \tag{2.19}$$

$$t_{24} = t_0 + \frac{(1-x)l_{34}}{v_{TW}} + \frac{l_{24}}{v_{TW}} \tag{2.20}$$

Here $l_{24}$ is the length of the DC transmission link $L_{24}$. By combining the above equations, we get

$$t_{42} - t_{24} = -\frac{l_{42}}{v_{TW}} \tag{2.21}$$

Also, $CT_{42}$ will see fault in reverse and $CT_{24}$ will see fault in forward direction for fault $F_1$. Therefore, the fault induced current TW at OCT $CT_{42}$ and $CT_{24}$ will have opposite polarity.

$$P_{CT_{24}}.P_{CT_{42}} = -1 \tag{2.22}$$

Therefore, the fault will be in the backward direction if the above two equations are satisfied.

The overall MTDC backup protection logic is shown in Fig. 2.4(b). After receiving a remote backup trip signal at DC substation $i$ from DC substation $(i-1)$ indicating fault in the forward direction, the logical AND gate 1 is activated if HDCCB breaker current is still non-zero (primary protection fails). Similarly, the logical AND gate 2 is activated if HDCCB breaker current is non-zero and remote backup trip signal is received from DC substation $(i+2)$ at DC substation $(i+1)$ indicating an external fault in the backward direction. The output of Logic AND gate 1 and 2 are given as input to logic AND gate 3 and the output of logic AND gate 3 is given as backup trip signal to HDCCB for DC transmission line between DC substation $i$ and $(i+1)$ with a coordinated time delay (CTD), taken as 2.23 ms in this study. During backup relay operation, the trip signal is delayed by CTD which accounts for 1 ms operating time of HDCCB, time taken by the traveling wave to travel the longest DC cable ($l_{34}/v_{TW} = 1.128ms \approx 1.13ms$) in the MTDC grid and 100 $\mu s$ of security margin.

### 2.3.3 Flowchart of proposed primary and backup protection scheme

The proposed primary and backup protection scheme for the MTDC system is being explained in the flowchart shown in Fig. 2.5. It can be briefly explained with the following steps –

1. DC pole currents are sampled at 500 kHz via current sensors at the DC transmission line terminal and sent to the local DC substation. After that DC pole currents are transformed to modal currents using (2.1).

2. Use the second-order MUDW technique from (2.9) to extract TW from mode-1 current at the DC cable terminal ends. If the MUDW output is greater than the predetermined threshold $\zeta$, then TW is detected. Afterwards, AT and polarity of the TW is calculated, otherwise go back to step 1. The magnitude of the threshold $\zeta$ is decided by the farthest

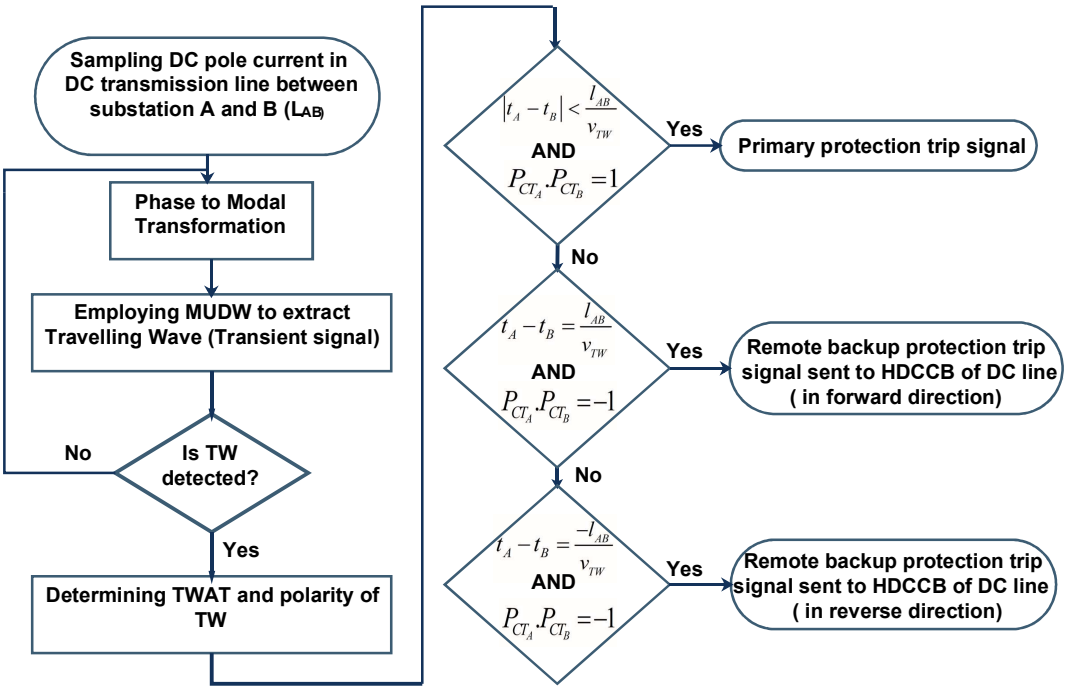


Figure 2.5: Flowchart of the proposed primary and backup MTDC protection scheme.

located, highest impedance DC fault in a worst noise measurement scenario. In the test MTDC system, the threshold $\zeta$ is found to be 0.001 to effectively provide primary and backup protection to MTDC grid.

3. If AT and polarity information of the first incident TW at DC terminal ends satisfies (2.13) and (2.14), then it is detected as an internal fault and the primary trip signal is sent to HDCCB of the primary DC transmission line. Otherwise go to step 4.

4. If (2.17) and (2.18) are satisfied for the polarity and AT of the first incident TW at DC cable ends, then it detects an external fault in the forward direction and a remote backup trip signal is sent to HDCCB of DC transmission line in the forward direction. Otherwise go to step 5.

5. If (2.21) and (2.22) are satisfied for the polarity and AT of the first incident TW at DC terminals, then it signifies a backward external fault and a remote backup trip signal is sent to HDCCB of DC transmission line in the backward direction.

## 2.4 Simulation result

The four-terminal test MMC-MTDC grid shown in Fig. 2.1 is modeled in PSCAD/EMTDC software. For test MTDC grid modeling, the continuous equivalent model for MMC converter and frequency-dependent distributed parameter models for DC cable are modeled in PSCAD software. The data generated from PSCAD is imported to MATLAB software for performance evaluation of the proposed primary and backup protection scheme. The TW velocity in DC cable is found to be 177.30 km/ms [98, 102]. A simulation step size of 2 $\mu s$ (sampling frequency of 500 kHz) is used for every simulation cases unless stated otherwise. For all the simulation cases, the measurement noises are contaminated with SNR of 30 dB, unless stated otherwise. Further, different case scenarios for evaluating the performance of proposed primary and backup protection schemes are discussed in following sections.

### 2.4.1 Effect of fault location on proposed protection scheme

The effectiveness of proposed primary and backup protection scheme is demonstrated by simulating a PP fault (with 50 Ω fault impedance) in DC cable $L_{34}$ at a distance of 80 km from DC substation 3. The time of fault occurrence was considered to be 0.8 s. The first incident TW and their corresponding MUDW based polarity and AT detection by OCTs $CT_{34}$, $CT_{43}$, $CT_{31}$, $CT_{13}$, $CT_{42}$, and $CT_{24}$ are shown in Fig. 2.6.

As observed from Fig. 2.6(b) and Fig. 2.6(c), the polarity of the first incident TW is same for $CT_{34}$ and $CT_{43}$, satisfying (2.14). On top of that, the AT difference between TW at OCT locations $CT_{34}$ and $CT_{43}$ is given as

$$|t_{34} - t_{43}| = |0.80044 - 0.80066| = 0.22 \text{ ms}$$

On the other hand, theoretically

$$\frac{l_{34}}{v_{TW}} = \frac{200}{177.3} = 1.128 \text{ ms}$$

Then, the $|t_{34} - t_{43}| < l_{34}/v_{TW}$ condition is confirmed. Since (2.13) and (2.14) are satisfied, therefore it will generate a primary trip signal for the associated HDCCB to DC cable $L_{34}$.

If the primary protection relay fails, then the first incident TW at OCT location $CT_{13}$ and $CT_{31}$ is plotted as shown in Fig. 2.6(e) and Fig. 2.6(f). As evident from Fig.

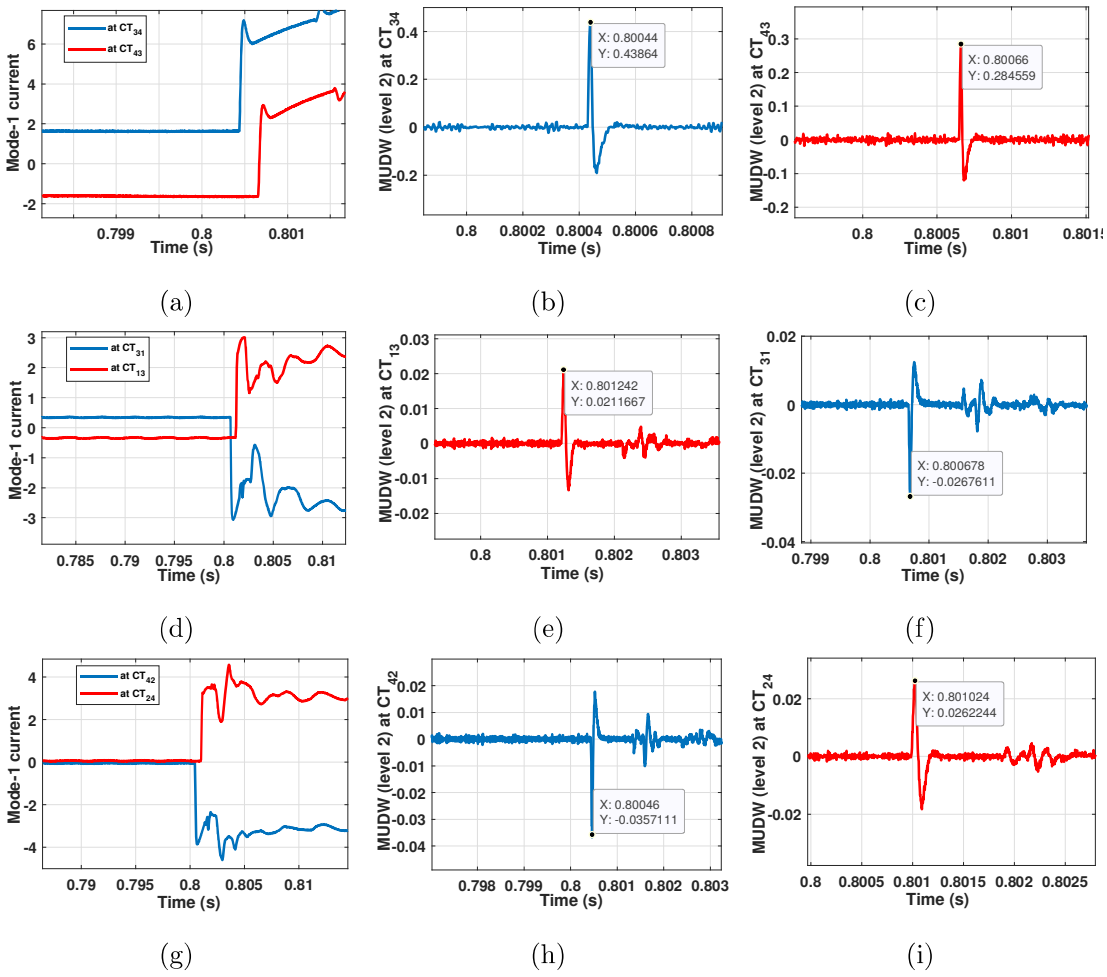


Figure 2.6: Performance of proposed MUDW based protection scheme (a) Mode-1 current at DC link $L_{34}$, (b) Polarity and AT of TW at $CT_{34}$, (c) Polarity and AT of TW at $CT_{43}$, (d) Mode-1 current at DC link $L_{13}$, (e) Polarity and AT of TW at $CT_{13}$, (f) , Polarity and AT of TW at $CT_{31}$, (g) Mode-1 current at DC link $L_{42}$, (h) Polarity and AT of TW at $CT_{42}$, (i) Polarity and AT of TW at $CT_{24}$.

2.6(e) and Fig. 2.6(f), the polarity of the TW is in contrast to each other, satisfying (2.18). Moreover, the AT difference between OCT location $CT_{13}$ and $CT_{31}$ is given as

$$t_{13} - t_{31} = 0.801242 - 0.800678 = 0.564 \text{ ms}$$

Also, theoretically

$$\frac{l_{13}}{v_{TW}} = \frac{100}{177.3} = 0.564 \text{ ms}$$

Since, (2.17) and (2.18) are confirmed. Therefore, it indicates that the fault is in the forward external direction. And consecutively it sends a remote backup trip signal to DC

Table 2.2: Effect of Fault Location on Proposed Protection Scheme for DC Fault in Cable $L_{34}$

| DC cable | Fault location (km) | Polarity $P_{CT_A}$ | Polarity $P_{CT_B}$ | $t_A - t_B$ (ms) | $l_A/v_{TW}$ (ms) | Zone identification |
|---|---|---|---|---|---|---|
| $L_{34}$ (Note: A=34, B=43) | 10 | + | + | 1.016 | 1.128 | $Z_{34}^{in}$ |
| | 100 | + | + | 0.000 | 1.128 | $Z_{34}^{in}$ |
| | 190 | + | + | 1.014 | 1.128 | $Z_{34}^{in}$ |
| $L_{13}$ (Note: A=13, B=31) | 10 | + | - | 0.564 | 0.564 | $Z_{13}^{fe}$ |
| | 100 | + | - | 0.564 | 0.564 | $Z_{13}^{fe}$ |
| | 190 | + | - | 0.564 | 0.564 | $Z_{13}^{fe}$ |
| $L_{42}$ (Note: A=42, B=24) | 10 | - | + | -0.564 | -0.564 | $Z_{42}^{be}$ |
| | 100 | - | + | -0.564 | -0.564 | $Z_{42}^{be}$ |
| | 190 | - | + | -0.564 | -0.564 | $Z_{42}^{be}$ |

Substation 3, which in turn uses backup protection logic shown in Fig. 2.4(b) to generate the backup trip signal for HDCCB with CTD.

Similarly, as observed in Fig. 2.6(h) and Fig. 2.6(i), the polarity of the first incident TW at the OCT location $CT_{42}$ and $CT_{24}$ are opposite to each other, which satisfies (2.22). Moreover, the AT difference between TW at the OCT location $CT_{42}$ and $CT_{24}$ is given as

$$t_{42} - t_{24} = 0.800046 - 0.801024 = -0.564 \text{ ms}$$

And, theoretically

$$\frac{-l_{42}}{v_{TW}} = \frac{-100}{177.3} = -0.564 \text{ ms}$$

Now, (2.21) and (2.22) is satisfied for the OCT location $CT_{42}$ and $CT_{24}$, which indicates that the fault is in the backward external direction and sends a remote backup trip signal to DC substation 4, which generates the backup trip signal for HDCCB using backup protection logic shown in Fig. 2.4(b).

To evaluate the effectiveness of different fault locations on the proposed primary and backup protection scheme, the PP fault (with 50 Ω fault impedance) is created at 10, 100,

190 km in DC cable $L_{34}$. The polarity information of the TW at the relay locations of all the DC cables will not change for the same fault type with varying fault locations, but the AT difference will definitely change. The AT differences of the first incident TW at both ends of the DC cable $L_{34}$, $L_{13}$, and $L_{42}$ are tabulated in Table 2.2. As evident from Table 2.2, the AT difference between OCT locations $CT_{34}$ and $CT_{43}$ is always less than the threshold $l_{34}/v_{TW}$ (1.128 ms). And the AT between OCT locations $CT_{13}$ and $CT_{31}$ is approximately equal to the threshold $l_{13}/v_{TW}$ (0.564 ms). Similarly, the AT between OCT location $CT_{42}$ and $CT_{24}$ is approximately equal to the threshold - $l_{42}/v_{TW}$ (-0.564 ms). Hence, it can be concluded that the proposed protection scheme correctly identifies the zones of the fault location, i.e.; internal zone, forward external zone, and backward external zone. After that, it accordingly generates primary and remote backup trip signals for the associated HDCCB ($CB_3$ and $CB_4$) of the DC line $L_{34}$.

### 2.4.2 Effect of noise on MUDW based TWAT extraction technique

The optical CTs (OCTs) and electrical potential transducers (EPTs) used to measure DC pole current and DC voltage in the MTDC transmission system may be susceptible to measurement noise. And the measurement noise may hinder the performance of the proposed protection scheme. According to the previous HVDC projects, the general signal-to-noise-ratio (SNR) content of a certain type of OCT and EPT measurement is found to be 34.9 dB [17]. In some HVDC projects, it also goes down to 30 dB SNR. To analyze the effect of noise on MUDW based TW polarity and AT detection, we have created a PP fault (with 70 Ω fault impedance) at 105 km distance from DC substation 3 in DC cable $L_{34}$ at a time instant of 1.5 s. The TW will travel further in the external DC cable $L_{42}$ in the forward direction (which will generate a remote backup trip signal for backward external fault in $L_{34}$), where TW will be significantly attenuated. Therefore, the performance of the MUDW technique to detect AT and polarity of noise-contaminated DC mode 1 signal by OCT $CT_{24}$ installed at the end of DC cable $L_{24}$ near DC terminal 2 is shown in Fig. 6. As evident from Fig. 2.7, that MUDW can effectively detect AT of the TW under no noise, 40- and 30-dB SNR noise level (worst noise contamination) to be 1.5011 s, 1.50109 s and 1.5011 s respectively. The detected polarity of TW is positive

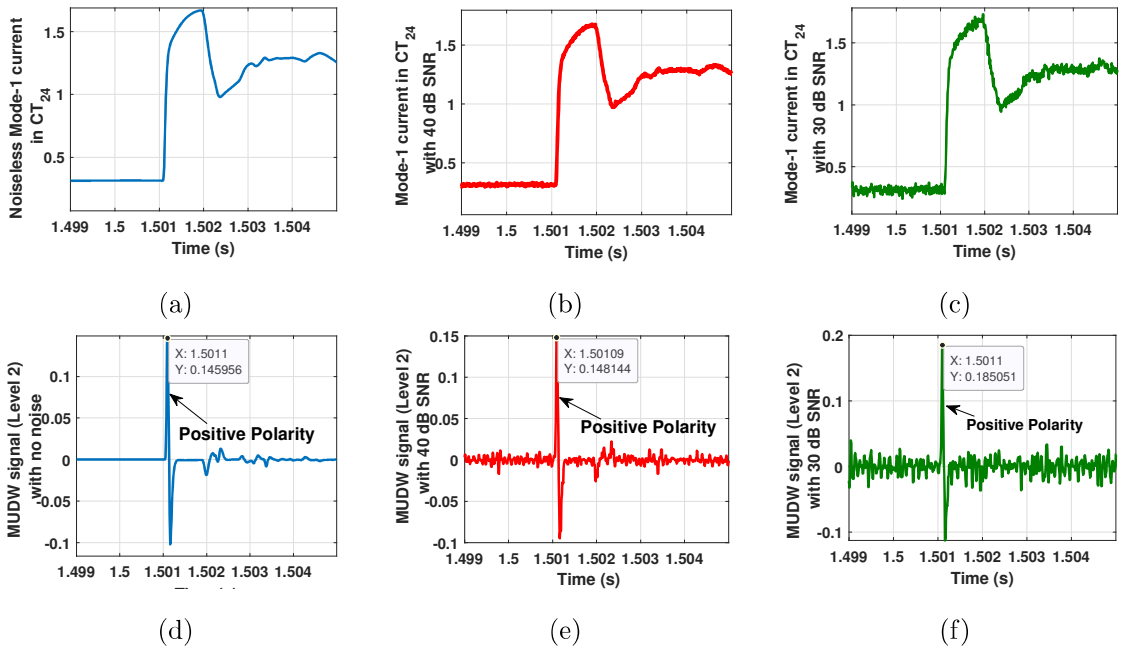


Figure 2.7: (a) Noiseless Mode-1 current signal in CT24, (b) Mode-1 current signal in $CT_{24}$ with 40 dB SNR, (c) Mode-1 current signal in $CT_{24}$ with 30 dB SNR, (d) MUDW output for noiseless signal in $CT_{24}$, (e) MUDW output for signal with 40 dB SNR in $CT_{24}$, (f) MUDW output for signal with 30 dB SNR in $CT_{24}$.

for all noiseless and noise-contaminated signals.

### 2.4.3 Effect of fault impedance and measurement noise on MUDW based primary and backup protection scheme

To investigate the effect of fault impedance on the MUDW based AT and polarity detection of TW, a PP fault in DC cable $L_{34}$ with fault impedance 10 Ω, 50 Ω, and 100 Ω is created at 50 km distance from DC substation 3. The fault-induced TW will travel to the neighbouring DC cable (DC cable $L_{34}$ and $L_{42}$), where the TW will be further attenuated by the DC cable, which may challenge the ability of polarity and AT detection of TW in the neighbouring line. Therefore, the OCT $CT_{24}$ will be monitored for checking the ability of MUDW based polarity and AT detection of the TW. As evident from Fig. 2.8, the $CT_{24}$ near DC substation 2 can comfortably detect polarity (positive polarity) and AT (0.801408 ms) for the TW due to different fault impedance at DC cable $L_{34}$.

Although the MUDW technique can extract TW features for the fault impedance

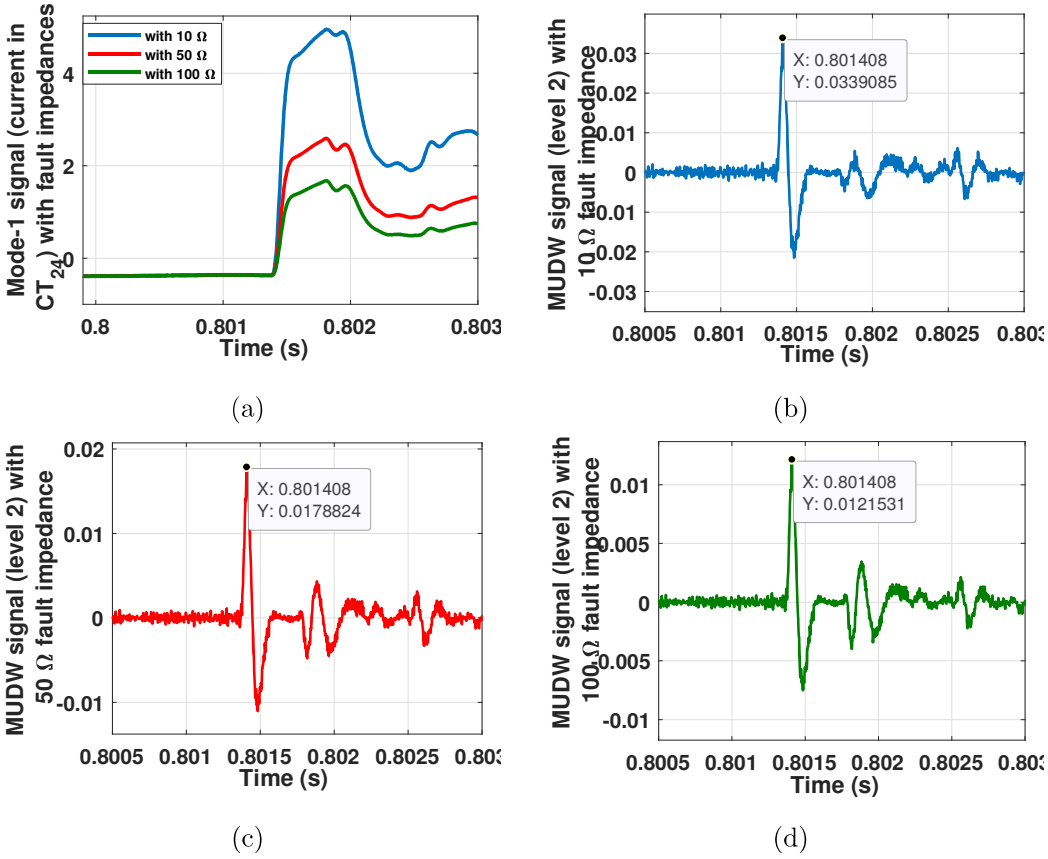


Figure 2.8: (a) Mode-1 current signal in $CT_{24}$ with 10 Ω, 50 Ω and 100 Ω fault impedance, (b) MUDW signal output with 10 Ω fault impedance, (c) MUDW signal output with 50 Ω fault impedance, (d) MUDW signal output with 100 Ω fault impedance.

more than 100 Ω in internal zone (primary protection zone), but the fault induced TW will be further attenuated while traveling to external neighbouring DC cable and TW feature extraction for forward and backward external zone (backup protection zone) will be limited to fault impedance up to 100 Ω only. Therefore, the proposed MUDW based primary protection scheme is applicable for fault impedance more than 100 Ω, but the proposed MUDW based backup protection scheme is limited for fault impedance up to 100 Ω only.

To verify the performance of proposed primary and backup protection scheme against different fault resistance and measurement noise, a DC fault with 10 Ω, 50 Ω and 100 Ω fault resistance is simulated at 50 km distance from DC substation 3 in DC cable $L_{34}$ under the measurement noise of 30 dB. The TW arrival time and zone identification by the proposed scheme is tabulated in Table 2.3. And it is evident that the proposed scheme

correctly identifies the internal, forward external and backward external zone, which helps the proposed scheme to provide secured primary and backup protection to DC cable $L_{34}$.

Table 2.3: Effect of measurement noise and Fault impedance on Proposed Protection Scheme for DC Fault at 50 km from DC Bus 3 in Cable $L_{34}$

| DC cable | Noise (dB) & Fault type (Ω) | Polarity $P_{CT_A}$ | Polarity $P_{CT_B}$ | $t_A - t_B$ (ms) | $l_A/v_{TW}$ (ms) | Zone identification |
|---|---|---|---|---|---|---|
| $L_{34}$ (Note: A=34, B=43) | 30 & 10 | + | + | 0.564 | 1.128 | $Z_{34}^{in}$ |
| | 30 & 50 | + | + | 0.564 | 1.128 | $Z_{34}^{in}$ |
| | 30 & 100 | + | + | 0.563 | 1.128 | $Z_{34}^{in}$ |
| $L_{13}$ (Note: A=13, B=31) | 30 & 10 | + | - | 0.564 | 0.564 | $Z_{13}^{fe}$ |
| | 30 & 50 | + | - | 0.564 | 0.564 | $Z_{13}^{fe}$ |
| | 30 & 100 | + | - | 0.564 | 0.564 | $Z_{13}^{fe}$ |
| $L_{42}$ (Note: A=42, B=24) | 30 & 10 | - | + | -0.564 | -0.564 | $Z_{42}^{be}$ |
| | 30 & 50 | - | + | -0.564 | -0.564 | $Z_{42}^{be}$ |
| | 30 & 100 | - | + | -0.564 | -0.564 | $Z_{42}^{be}$ |

### 2.4.4 Effect of fault types on proposed protection scheme

The effectiveness of the proposed protection scheme is demonstrated for PP fault in the previous subsection. To demonstrate the performance of the proposed primary and backup protection scheme against different types of fault, a PP, PPG and NPG fault (with 100 Ω) is simulated at a distance of 80 km from DC substation 3 in DC cable $L_{34}$. The AT and polarity information of the first incident TW at DC terminal ends of the DC cable $L_{34}$, $L_{13}$ and $L_{42}$ is tabulated in Table 2.4. As evident from Table 2.4, the polarity and At information of the first incident TW correctly identifies fault zones, i.e.; internal zone, forward external zone and backward zone. It helps the proposed protection scheme to send the trip signal to associated HDCCB for primary protection and trip signal with CTD delay for backup protection.

Table 2.4: Effect of Fault Location on Proposed Protection Scheme for DC Fault in Cable $L_{34}$

| DC cable | Fault type | Polarity $P_{CT_A}$ | Polarity $P_{CT_B}$ | $t_A - t_B$ (ms) | $l_A/v_{TW}$ (ms) | Zone identification |
|---|---|---|---|---|---|---|
| $L_{34}$ (Note: A=34, B=43) | PPG | + | + | 0.225 | 1.128 | $Z_{34}^{in}$ |
| | NPG | + | + | 0.225 | 1.128 | $Z_{34}^{in}$ |
| | PP | + | + | 0.225 | 1.128 | $Z_{34}^{in}$ |
| $L_{13}$ (Note: A=13, B=31) | PPG | + | - | 0.564 | 0.564 | $Z_{13}^{fe}$ |
| | NPG | + | - | 0.564 | 0.564 | $Z_{13}^{fe}$ |
| | PP | + | - | 0.564 | 0.564 | $Z_{13}^{fe}$ |
| $L_{42}$ (Note: A=42, B=24) | PPG | - | + | -0.564 | -0.564 | $Z_{42}^{be}$ |
| | NPG | - | + | -0.564 | -0.564 | $Z_{42}^{be}$ |
| | PPG | - | + | -0.564 | -0.564 | $Z_{42}^{be}$ |

### 2.4.5 Effect of sampling frequency on proposed protection scheme

A PP fault (with fault impedance of 50 Ω) is created in DC cable $L_{34}$ with varying distances from 5 km to 195 km with a step size of 5 km. The test case is simulated with the different sampling frequencies of 1 MHz, 800 kHz, and 500 kHz. The sampling frequency will not affect the polarity information of the TW, but it will surely affect the AT information. Therefore, the AT differences of the first incident TW at both ends of the DC cable $L_{34}$, $L_{13}$ and $L_{42}$ for different sampling frequency is plotted in Fig. 2.9. As evident from Fig. 2.9(a), (13) is satisfied for sampling frequency ranging from 500 kHz -1000 kHz and the fault is identified to be in the internal zone (primary protection activates). In low sampling frequency simulation cases, the time resolution is also lower. For example, the time resolution is 2 $\mu$s with 500 kHz, and therefore, the AT difference threshold for internal, forward external, and backward external zone threshold will have a buffer threshold, instead of a single threshold, to correctly identify the fault zone even with low sampling frequency. In Fig. 2.9(b) and Fig. 2.9(c), the buffer threshold is (0.564±0.004 ms) and (-0.564±0.004 ms) respectively, where (0.002 ms) is the lowest time

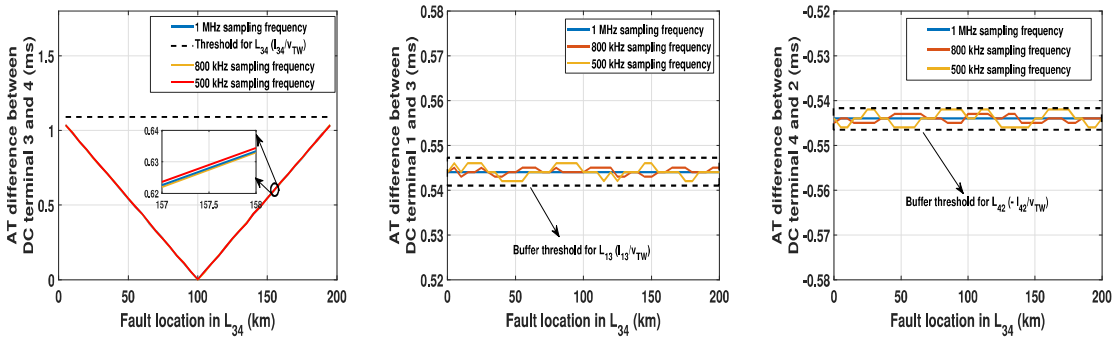


(a) (b) (c)

Figure 2.9: Effect of sampling frequency on AT of $F_1$ induced TW in (a) DC Link $L_{34}$, (b) DC Link $L_{13}$, (c) DC Link $L_{42}$.

resolution corresponding to the lowest sampling frequency (500 kHz). As evident from Fig. 2.9(b) and Fig. 2.9(c), (2.17), and (2.21) are satisfied and the proposed protection scheme correctly identifies forward and backward external zone of fault location. With buffer threshold mechanism, the proposed protection scheme correctly identifies the zone of fault location, which in turn generates primary and backup trip signals for the associated HDCCB ($CB_3$ and $CB_4$) of the DC line $L_{34}$.

### 2.4.6 Comparative analysis

In this section, the proposed MUDW based protection scheme is compared with one of the existing MMG-based MTDC protection schemes in the literature [17]. First, the superiority of the MUDW over MMG signal processing technique to extract polarity and AT of the noise-contaminated TW is already shown in Fig. 2.3. To compensate for the superior performance of MUDW over MMG, the MMG based protection technique uses MM based opening closing (OC) filter and finite impulse response (FIR) based low pass filter to filter out white noise and abnormal spike from the signal but it will add significant time delay [17], which will hinder fast protection requirement of MTDC grid. In comparison, the MUDW has better quality filtering than the MMG technique with a lesser time delay. The MMG-based protection scheme uses directional startup criteria and SATD between mode-0 and mode-1 TW to detect if the fault is internal or external. As explained in section 2.3.1, the mode-1 signal can be used to detect PP fault induced TW but the mode-0 signal cannot detect PP fault induced TW. Therefore, SATD between

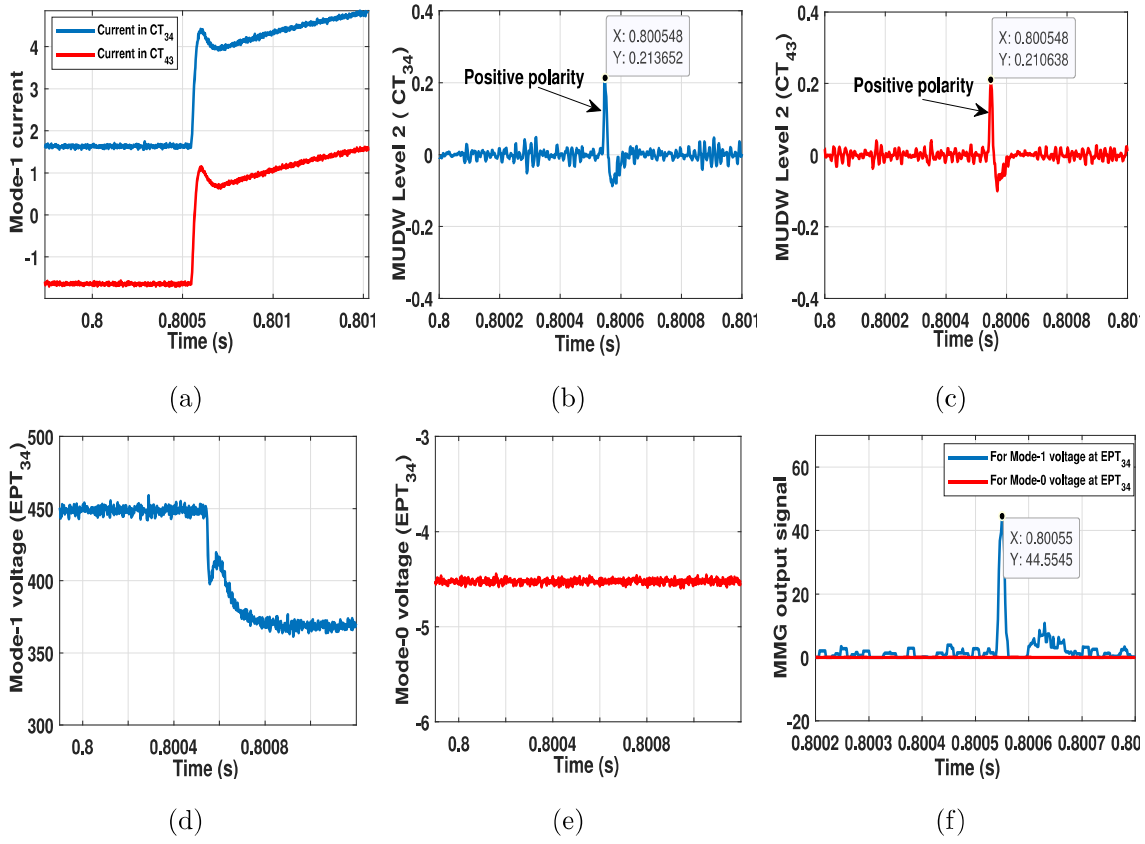


Figure 2.10: Comparison of Proposed MUDW protection scheme with MMG based protection scheme (a) Mode-1 current at both end of DC link $L_{34}$, (b) Polarity and AT of TW at $CT_{34}$, using MUDW (c) Polarity and AT of TW at $CT_{43}$ using MUDW, (d) Mode-1 voltage at $EPT_{34}$, (e) Mode-0 voltage at $EPT_{43}$, (f) SATD difference between AT of TW between mode-1 and mode-0 signal using MMG technique.

mode-0 and mode-1 TW cannot detect PP fault, and hence it will fail to detect PP fault in the MTDC transmission system. But the proposed protection scheme can effectively detect all fault types in the MTDC grid.

To compare the performance of the proposed MUDW based protection scheme and MMG-based protection scheme, a PP fault (with 100 Ω fault impedance and 35 dB noise) is created in the middle of the DC cable $L_{34}$ at 0.8 s time instant and its associated figures are plotted in Fig. 2.10. As evident from Fig. 2.10(b) and Fig. 2.10(c), $|t_{34} - t_{43}| = |0.800548 - 0.800548| = 0.000$ ms for the proposed protection scheme which is well below the threshold $l_{34}/v_{TW} = 1.128ms$ and also $P_{CT_{34}}.P_{CT_{43}} = 1$ , which identifies that the fault lies in the internal zone and the primary trip signal is sent to the associated HDCCB.

Table 2.5: Comparative analysis with existing primary and backup protection scheme

| **Backup protection category** | **Feature and challenges** |
|---|---|
| Transient based [29] | • Quickest change detection (QCD) signal processing technique is quite sensitive to high impedance faults.<br>• The performance of QCD based technique is also very limited under worst measurement noise. |
| Machine Learning-based [26, 27] | • Training of the system is required. Since fault records are not always sufficient (or sometimes not available at all) the training is usually implemented by simulation based iterative studies. This could raise concerns with regards to the reliability of the system training.<br>• Requirement of detailed system modelling, intensive training for different fault conditions, limited scalability, system topology dependence. |
| Proposed technique (TW based) | • The TWAT and polarity principle is used for primary and backup protection logic for DC fault in the MTDC grid.<br>• Training of the system is not required for TW based scheme. Therefore, it is highly reliable.<br>• The proposed TWAT based protection scheme is also resilient to measurement noise up to 30 dB. |

For the MMG-based protection scheme, the TW is absent in the mode-0 signal as shown in Fig. 2.10(f), therefore the SATD cannot be determined for the PP fault in the MMG-based MTDC protection scheme. The brief comparison of the proposed scheme against literature work is also tabulated in the following Table 2.5.

## 2.5 Summary

The MUDW technique is used to detect AT and polarity of the first incident TW at both terminals of the DC transmission line. After that, the concept of AT and polarity information of the first TW at both ends of the DC transmission line is used to create three different zones. i.e.; internal zone, forward external zone, and backward external zone. If a fault lies in the internal zone, then a primary trip signal is sent to HDCCB associated with the DC transmission line. But, if the fault lies in forward and backward external direction, then a remote backup trip signal with a CTD delay is sent to HDCCB in forward and backup direction respectively. The four-terminal MMC-MTDC test system is used to verify the effectiveness of the proposed protection technique. Numerous test cases have demonstrated the effectiveness of the proposed protection scheme under different fault impedance, fault location, fault type, noise contamination, and sampling frequency measurement.